Quaternary Science Reviews 215 (2019) 293–307

Contents lists available at ScienceDirect

Quaternary Science Reviews

journal homepage: www.elsevier.com/locate/quascirev

Oceanic and atmospheric modes in the Pacific and Atlantic Oceans since the Little Ice Age (LIA): Towards a synthesis

Keyan Fang [a, b, *], Deliang Chen [b], Liisa Ilvonen [c, d], Leena Pasanen [c], Lasse Holmström [c], Heikki Seppä [d], Gang Huang [e, f], Tinghai Ou [b], Hans Linderholm [b, g]

[a] Key Laboratory of Humid Subtropical Eco-geographical Process (Ministry of Education), College of Geographical Sciences, Fujian Normal University, Fuzhou 350007, China
[b] Regional Climate Group, Department of Earth Sciences, University of Gothenburg, Box 460 S-405 30 Gothenburg, Sweden
[c] Department of Mathematical Sciences, University of Oulu, Oulu, Finland
[d] Department of Geosciences and Geography, PO Box 64, 00014, University of Helsinki, Helsinki, Finland
[e] State Key Laboratory of Numerical Modeling for Atmospheric Sciences and Geophysical Fluid Dynamics, Institute of Atmospheric Physics, Chinese Academy of Sciences, Beijing 100029, China
[f] University of Chinese Academy of Sciences, Beijing 100049, China
[g] Department of Geography, University of Cambridge, Cambridge, CB2 3EN, UK

ARTICLE INFO

Article history:
Received 8 November 2018
Received in revised form
9 April 2019
Accepted 19 May 2019
Available online 4 June 2019

Keywords:
Oceanic and atmospheric mode
Climate reconstruction
ENSO
PDO
AMO

ABSTRACT

Understanding the variability of the oceanic and atmospheric modes from the Little Ice Age (LIA, ~1250–1850) to the present can help evaluate their behaviors under future warming scenarios. Numerous proxy-based reconstructions of the oceanic and atmospheric modes were presented. It is highly needed for a synthesis study to evaluate the existing reconstructions of the dominant oceanic and atmospheric modes since the LIA. We found that the El Niño-Southern Oscillation (ENSO) reconstructions are only robust on interannual and interdecadal scales, while the reconstructed Pacific Decadal Oscillation (PDO) and Atlantic Multi-decadal Oscillation (AMO) are robust on multi-decadal (50–100 years) timescales. We generated synthesized ENSO, PDO and AMO reconstructions as the average of the existing reconstructions on the most suitable timescales identified using timescale dependent correlation methods. In the 20th century, the interannual variability and periodicity of the ENSO and the multi-decadal periodicity of the PDO and AMO were most pronounced. The ENSO shows the strongest multi-decadal periodicity from mid-18th century onwards, while the multi-decadal periodicity of the PDO and AMO was particularly low in the 18th century. Multi-decadal variations of the AMO showed a prompt and positive response to solar irradiation, while the ENSO showed a lagged and negative response to solar irradiation from the 18th century to the present.

1. Introduction

Climate changes on interannual (1–10 years), interdecadal (herein 10–50 years) and multi-decadal (50–100 years) scales have received special attention from both the scientific community and the general public, as these timescales are relevant when considering climate change mitigation strategies and sustainable development (Stocker et al., 2013). Oceanic and atmospheric modes, such as the El Niño-Southern Oscillation (ENSO) and the Atlantic Multi-decadal Oscillation (AMO), are the main regulators of climate variability on these timescales. These modes are, in turn, often modulated by external forcings, such as solar irradiance, leading to non-linear and indirect relationships between external forcings and climate (Knudsen et al., 2014). Moreover, oceanic and atmospheric modes not only influence their core regions, where they are defined, but also can influence distant regions via teleconnections.

Owing to the importance of dynamic climate modes in the Earth's climate system, a number of indices have been defined that encapsulate teleconnections or particular states of the oceanic or atmospheric systems (Allan et al., 1996; Mantua and Hare, 2002; Schlesinger and Ramankutty, 1994; Walker and Bliss, 1932), and the list is constantly growing. On interannual scales, ENSO in the Pacific Ocean affects the climate in tropical western and eastern Pacific

* Corresponding author. Key Laboratory of Humid Subtropical Eco-geographical Process (Ministry of Education), College of Geographical Sciences, Fujian Normal University, Fuzhou 350007, China.
E-mail address: kujanfang@gmail.com (K. Fang).

https://doi.org/10.1016/j.quascirev.2019.05.014
0277-3791/

Ocean and surrounding land areas, but is also the major regulator of interannual climate variability across the globe (Allan et al., 1996; Li et al., 2013; Liu et al., 2017). On interdecadal and multi-decadal timescales, global climate is influenced by the Pacific Decadal Oscillation (PDO) (Dai et al., 2015; Mantua and Hare, 2002) of the Pacific Ocean, and the AMO (Schlesinger and Ramankutty, 1994; Wang et al., 2017) in the Atlantic Ocean.

The brevity of the instrumental data used to derive indices representing these modes limits our ability to detect possible regime shifts of these modes, and their relationships with regional climates. That is particularly true for long timescales and before the industrial era. Proxy-based reconstructions of the past millennium provide potential keys to study long-term climate variability on different timescales, and place the current climate in a longer context, including the pre-industrial period (PAGES 2k Consortium, 2013). A large number of reconstructions of oceanic and atmospheric modes have been presented using high-resolution proxies, such as tree rings and corals (Cook et al., 2004; D'Arrigo and Wilson, 2006; Fang et al., 2014; Li et al., 2013; Liu et al., 2017; MacDonald and Case, 2005; Villalba et al., 2012; Wang et al., 2017; Wilson et al., 2010).

Proxy-based reconstructions of oceanic and atmospheric modes are generally based on the teleconnections between regional climate affecting the proxies and the climate mode, which often defined to the ocean (Cook et al., 2002). However, the teleconnection between regional climate and climate modes may vary through time. That is, the teleconnected region in instrumental period may shift to other regions in historical periods. Indeed, relative to the temperature and precipitation reconstructions, the reconstructions of a given oceanic and atmospheric mode often show many disagreements in historical periods. In addition, the proxies are often more sparsely distributed in the earlier periods and there are uncertainties for each proxy records. Thus it is highly needed to evaluate and identifying the robust reconstructions on different timescales. The Little Ice Age (LIA), spanning from ~1250 to 1850, was the coldest period of the past two millennia (Stocker et al., 2013). It is important to study the variability of oceanic and atmospheric modes from the LIA to present, the most pronounced warming trend over the past millennia (Stocker et al., 2013), which can help assess the behaviors of the climate modes under future warming scenarios.

Since ENSO, PDO, and the AMO are key modes exerting the strong influences on global climate from interannual and multi-decadal timescales, respectively, this study focuses on timescale-dependent comparisons of them and provides synthesis of these modes. The selection of the reconstructed modes and the analytical methods for the synthesis is presented in section 2. The ENSO is analyzed in section 3, the PDO in section 4 and the AMO in section 5. The syntheses are discussed and summarized in section 6.

2. Data and methods

2.1. Reconstruction

All the reconstructions of the ENSO, PDO, and the AMO, freely available from the National Climate Data Center (NCDC; https://www.ncdc.noaa.gov/), were used in this study. As our study focuses on continuous series, event reconstructions of the ENSO from NCDC (Gergis and Fowler, 2009) were not included. Since this study quantitatively assessed the coherence among reconstructions, the reconstructions without data availability were not included. To make meaningful comparisons, we selected those reconstructions which differed in terms of proxy locations or proxy types used, and if the same proxy data were used in two reconstructions, we chose the updated one. For example, one early ENSO reconstruction using tree rings from subtropical North America (D'Arrigo et al., 2005) was updated by a latter reconstruction (Cook et al., 2008), so we used the latter one. The proxy data linked to the reconstructions are presented in the following sections.

2.2. Methods

To evaluate the timescale dependent correlations between different reconstructions of the same climate mode, we used the Pearson correlation, Wavelet Coherence (WTC), and scale space multiresolution correlation analyses. Pearson correlations were calculated for the original, high-pass ($f > 0.1$) and low-pass ($f < 0.1$) filtered data. The time-series of a given frequency range was created by using Gaussian filtering (Ghil et al., 2002; Park, 1992). An example to illustrating the use of this method is shown in Fig. S1. The WTC (toolbox available at: http://www.pol.ac.uk/home/research/waveletcoherence/) is an ideal tool to transform time-series into a time-frequency plane and then measure local correlations (Grinsted et al., 2004; Torrence and Compo, 1998). This allows for investigations of any time-varying and timescale dependent correlations between time series. The WTC can also detect relative phase relationships.

A recently proposed method for the detection of time-varying and timescale dependent correlations is scale space multi-resolution correlation analysis (Pasanen and Holmström, 2017). This technique is an example statistical scale space methodology (Chaudhuri and Marron, 1999), a family of techniques that has been successfully applied in various scientific fields, including climatology (Fang et al., 2018a; Holmström and Pasanen, 2017). In the scale space multiresolution correlation analysis, two time series are first decomposed to several additive multiresolution components of different timescales. The number of components and their time scales are determined by the data and not assigned a priori. For each pair of the naturally identified components, the scale space method allows localized correlations to be calculated for a range of time window widths. Hence, the extracted components and their correlation maps provide detailed, and easily interpretable, information about scale and time dependent correlations between the time series.

We only the synthesized the climate modes of certain timescales, which had coherent variations. The reconstructions were considered robust at a given timescale, if, based on the timescale dependent correlation tools presented above, they appeared to match at that timescale. We then applied Gaussian filtering to extract the time series to produce synthesized series by averaging over the identified timescales. Since the mean and variances of the reconstructed series of varying lengths used for averaging could be different, we keep all the series with the same mean and variance during their common periods before averaging. In application, we first ensure the reconstructed series having the same mean and variance during their most replicated period, and then keep the second most replicated period having the same mean and variance. In so doing, we step by step adding the longer series into the synthesized series. It is reasonable to generate the synthesis via averaging reconstructions that were based on independent proxies from different locations and showed coherent variations with each other. This application is similar to the reconstructions using sensitive proxies of multiple locations, which was also applied in other studies (McGregor et al., 2010). The time-varying periodicities were evaluated by wavelet analysis based on a Morlet function, which can transform the time series into a time-frequency profile (Torrence and Compo, 1998). The significance test was based on a red noise background.

3. ENSO

3.1. ENSO reconstructions

ENSO is a coupled ocean-atmospheric pattern, including an oceanic component, defined based on SST in eastern Pacific Ocean,

and an atmospheric component of the Southern Oscillation that is defined as the pressure difference in the subtropical central and western Pacific Ocean (Allan et al., 1996). The frequently used ENSO indices (Niño1+2, Niño3, Niño3.4, Niño4) were defined based on the mean SST from eastern to western parts of the eastern and central Pacific Ocean (Allan et al., 1996). ENSO dominates the interannual climate variability over subtropical North America and Asian monsoonal areas as well as distant regions of the pan-Pacific areas (Li et al., 2013).

As shown in Fig. 1 and Table 1, the ENSO reconstructions analyzed herein include one based on proxies from the western equatorial Pacific Ocean (Wilson et al., 2010), two using tree rings from subtropical North America (Cook et al., 2008; Li et al., 2011), one using proxies from both the western equatorial Pacific Ocean and subtropical North America (Stahle et al., 1998), and three using proxies from multiple regions from low to high latitudes (Braganza et al., 2009; Li et al., 2013; McGregor et al., 2010).

The reconstructions by Wilson et al. (2010) and McGregor et al. (2010) used proxies from the eastern equatorial Pacific Ocean, the core areas to define the ENSO. Although ENSO is defined to eastern equatorial Pacific Ocean, the reconstruction based on proxies from western equatorial Pacific Ocean is more stable over time (Stahle et al., 1998; Wilson et al., 2010). This may be because of a reduced quality of the proxies from eastern equatorial Pacific Ocean. The reconstructions by Stahle et al. (1998), Braganza et al. (2009), Wilson et al. (2010), McGregor et al. (2010) and Li et al. (2013). Subtropical North America is close to the eastern equatorial Pacific Ocean and its winter-spring precipitation is strongly controlled by the ENSO. The reconstructions by Cook et al. (2002), McGregor et al. (2010), Li et al. (2011) and Li et al. (2013) used similar tree rings in this region. Apart from the eastern and western equatorial Pacific Oceans and their vicinity, ENSO can exert influence over remote areas via teleconnections, thus proxies from these regions were used for reconstructions. For example, McGregor et al. (2010) and Li et al. (2013) used proxy data from central Asia and central part of South America. Braganza et al. (2009), McGregor et al. (2010) and Li et al. (2013) used proxies from and north parts of South America. Detailed descriptions of these reconstructions were seen in the Appendix.

3.2. Synthesis of the ENSO reconstructions

As shown in Table 2, the ENSO reconstructions are highly correlated, except for the two reconstructions by Wilson et al. (2010). In general, the correlations between different reconstructions are higher on interannual timescale than on long timescale. This agrees with the fact that the ENSO is the major regulator in interannual climate variability (Allan et al., 1996). The average of inter-correlations with the reconstruction by McGregor et al. (2010) is the highest on both short and long timescales (Table 2). This is reasonable because that this reconstruction is the PC1 of many reconstructions. The average of the inter-correlations with the reconstruction by Braganza et al. (2009) is the second highest only on long ($f < 0.1$) timescales. This may indicate that the proxies used in the reconstruction by Braganza et al. (2009) were derived from locations (New Zealand, subtropical North America and South America) that more closely capture the long-term changes of the ENSO.

We calculated WTC for all pairs (Figs. S2, S3 and 2). The correlations on multi-decadal timescales are more significant among the reconstructions by Braganza et al. (2009), McGregor et al. (2010), Stahle et al. (1998) and Wilson et al. (2010), which were selected and shown in Fig. 2. The WTC analyses generally agree with the Pearson correlations (Table 2) and suggest that the ENSO reconstructions by Braganza et al. (2009) and McGregor et al. (2010) have close matches from short to long timescales (Fig. 2a). For the generation of a synthesized ENSO, we did not use the reconstruction by McGregor et al. (2010) because it has many overlapping proxies with the rest and it is highly correlated with the reconstruction by Braganza et al. (2009) and thus can be replaced by the latter one. On multi-decadal timescales, we found close matches between the ENSO reconstructions by Braganza et al. (2009), Stahle et al. (1998) and Wilson et al. (2010) as indicated by high correlations on these timescales (Fig. 2b, c and 2d).

Although the reconstruction by Wilson et al. (2010) has poor matches with others on interannual timescales, it has close matches with other reconstructions on multi-decadal scales. Different from the other reconstructions mainly based on tree rings, the ENSO reconstructions by Wilson et al. (2010) were mainly

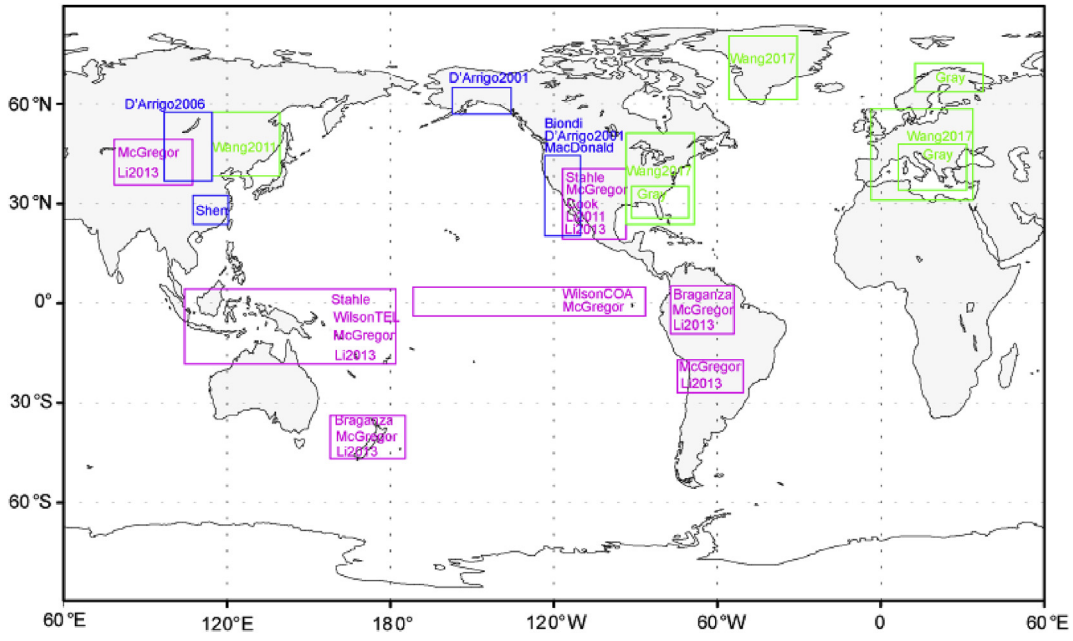

Fig. 1. Map of the locations of the proxy data used for the reconstructions of the (purple square) El Niño-Southern Oscillation (ENSO), the (blue square) Pacific Decadal Oscillation (PDO), and the (green square) Atlantic Multidecadal Oscillation (AMO). The rectangular indicate the range of locations of the proxy data used for each reconstruction. That is, boundaries of the rectangular are the latitudinal and longitudinal limits of the locations of the proxy data. The codes of the reconstructions are shown in Tables 1, 3 and 5. (For interpretation of the references to color in this figure legend, the reader is referred to the Web version of this article.)

Table 1
Metadata of the reconstructed El Niño-Southern Oscillation (ENSO) by Stahle et al. (1998) (Stahle), Cook et al. (2008) (Cook), Braganza et al. (2009) (Braganza), McGregor et al. (2010) (McGregor), Wilson et al. (2010) (WilsonCOA and WilsonTel), Li et al. (2011) (Li 2011), and Li et al. (2013) (Li 2013). More detailed introductions on these reconstructions were seen in the Appendix entitled as "Description of the ENSO reconstructions".

Code	Var.	Data source	Exp. var.	Method	Span	Reference
Stahle	Dec.–Jan.	Tree rings from Indonesia, North America and tropical ice cores and corals	53%	4 PCs	1706–1977	Stahle et al. (1998)
Cook	Dec.–Feb.	Tree rings from Mexico and Texas	N/A	2 PCs	1300–2006	Cook et al. (2008)
Braganza	year	Tree rings and ice cores from New Zealand, subtropical North America and South America	48%	Mean	1525-1982	Braganza et al. (2009)
McGregor	year	Tree rings, corals and ice cores from western and eastern Pacific Ocean, Indian Ocean, Asia, subtropical North America and South America	64%	PC1	1650–1977	McGregor et al. (2010)
Wilson	year	Tree rings, corals and ice cores from the tropics (30°S- 30°N)	63%	2 PCs	1540–1998	Wilson et al. (2010)
Li2011	Jan.–Mar.	Southwestern North America	25%	PC1	900–2002	Li et al. (2011)
Li2013	Nov.–Jan.	Asia, New Zealand, North and South America	64%	PC1	1301–1992	Li et al. (2013)

Table 2
Correlations between the raw/high-passed ($f > 0.1$)/low-passed ($f < 0.1$) El Niño-Southern Oscillation (ENSO) reconstructions. The ENSO and Pacific Decadal Oscillation (PDO) and Atlantic Multi-decadal Oscillation (AMO) have dominant timescales varying from short to long periods. The selection of the cutoff frequency at $f = 0.1$ is a tradeoff to facilitate comparisons of the correlations between all the three modes. The codes of the ENSO reconstructions are shown in Table 1.

Code	Cook	Braganza	McGregor	Wilson COA	Wilson TEL	Li2011	Li2013
Stahle	0.73/0.75/0.65	0.65/0.67/0.69	0.86/0.89/0.78	0.24/0.23/0.34	0.32/0.33/0.36	0.67/0.69/0.73	0.61/0.64/0.49
Cook		0.68/0.66/0.73	0.86/0.87/0.81	0.29/0.12/0.27	0.34/0.35/0.31	0.64/0.70/0.58	0.57/0.61/0.40
Braganza			0.87/0.85/0.91	0.26/0.27/0.26	0.39/0.38/0.39	0.52/0.58/0.59	0.59/0.61/0.48
McGregor				0.36/0.33/0.44	0.42/0.41/0.44	0.68/0.74/0.64	0.67/0.71/0.51
Wilson COA					0.46/0.52/0.36	0.11/0.12/0.20	0.28/0.27/0.35
Wilson TEL						0.17/0.21/0.13	0.32/0.32/0.33
Li2011							0.45/0.48/0.48

based on coral records. Dating of some coral records might be less accurate than tree rings and thus the coral based ENSO reconstructions may have relatively low correlations with other ENSO reconstructions on interannual timescales but generally agree with the others on multi-decadal timescales. To further examine the timescale dependent-correlations, we calculated the scale space multiresolution correlations between the ENSO reconstructions by Wilson et al. (2010) and Braganza et al. (2009). The two ENSO reconstructions indeed have closer matches on interdecadal and multi-decadal timescales but not on interannual timescales (Fig. 3). This agrees well with the WTC analyses. Close matches between these ENSO reconstructions on multi-decadal scales suggest that the ENSO not only has strong interannual variability but also shows interdecadal and multi-decadal variability.

We generated a synthesized reconstruction from the average of the reconstructions with close matches from interannual to multi-decadal timescales. All the reconstructions on short timescales (<50 years) were averaged, except for the two from Wilson et al. (2010) (Fig. 4a). The ENSO time series representing longer variations (>50 years) was generated by averaging the multi-decadal

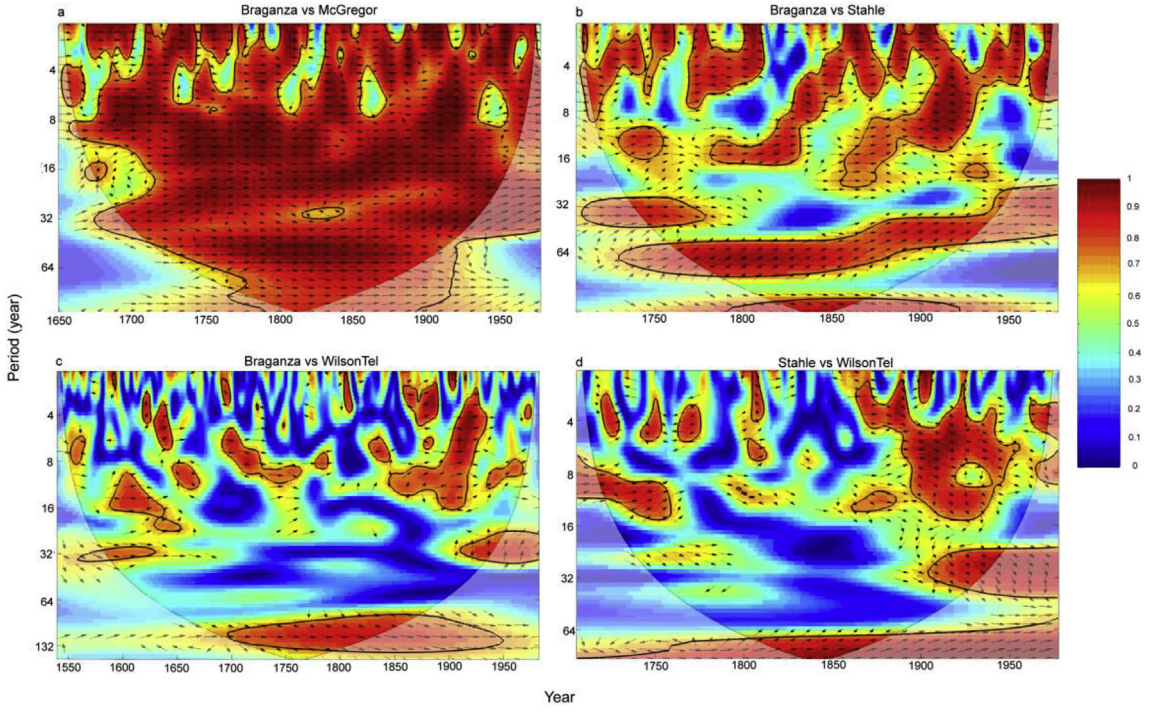

Fig. 2. Wavelet coherence (WTC) between pairs of the reconstructed El Niño-Southern Oscillation (ENSO) reconstructions. The WTC indicates the correlations instead of common powers between the target pairs. The arrows pointing right mean in-phase changes and pointing left indicate anti-phase changes. Significant correlations are indicated by contours. The cone of influence is narrower at longer timescales. The codes of the ENSO reconstructions are shown in Table 1.

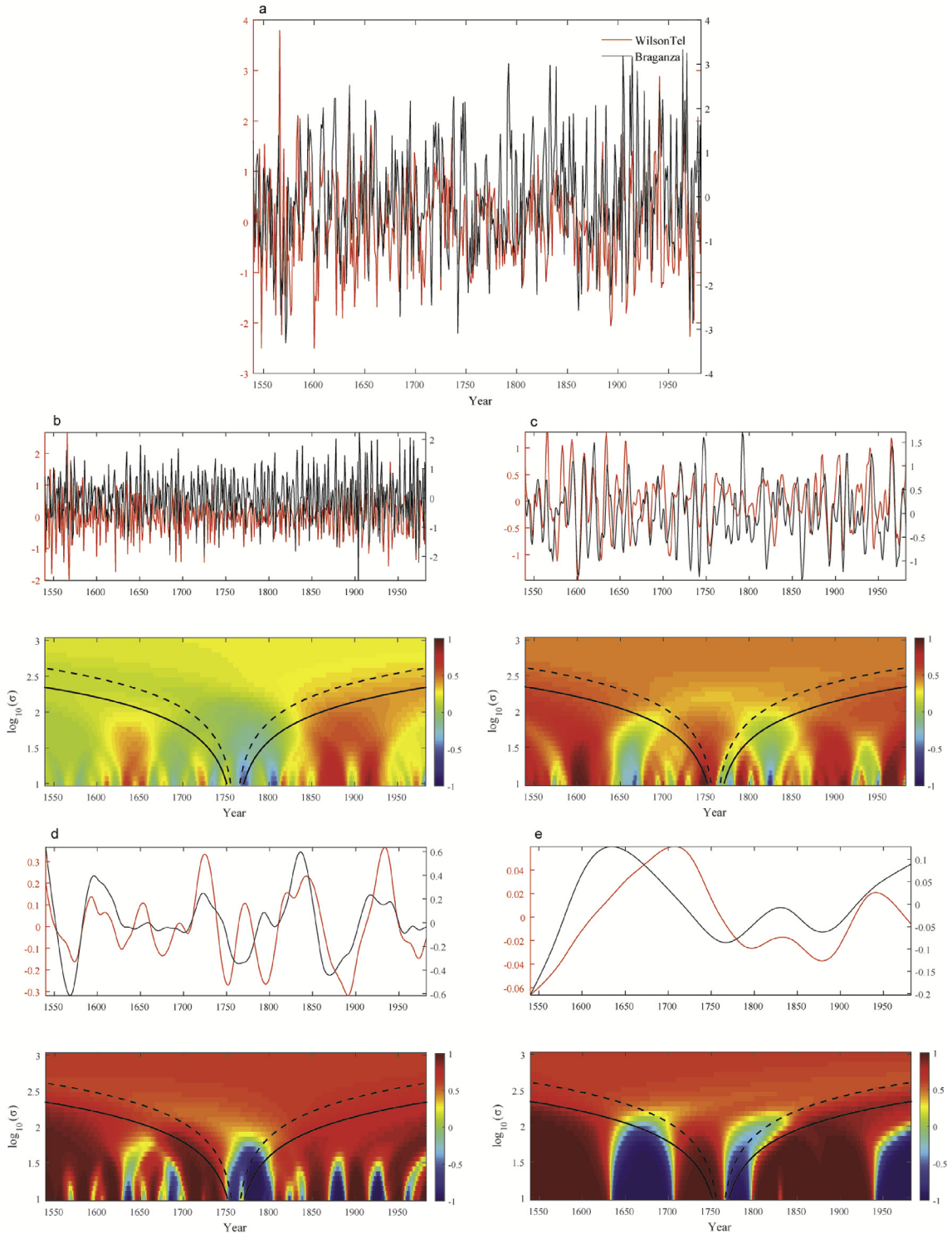

Fig. 3. Map of the scale space correlations between the reconstructed El Niño-Southern Oscillation (ENSO) by Braganza et al. (2009) (Braganza) and Wilson et al. (2010) (WilsonTel). The time series components and the correlations from short to long timescales were calculated in consecutive panels. In the correlation map, the vertical axis represents the logarithm of the parameter σ that indicates the sliding window width used in the local correlation (see further details in Pasanen and Holmström, 2017). The horizontal space between the solid lines visualizes the width of the sliding-window kernel and the dashed lines indicate the width of the interval where the kernel height has decreased to 50% of its maximum value. The color of each pixel indicates the value of the local correlation. (For interpretation of the references to color in this figure legend, the reader is referred to the Web version of this article.)

variations of the reconstructions by Stahle et al. (1998), Braganza et al. (2009), and Wilson et al. (2010) (Fig. 4b). It is reasonable to generate the synthesized ENSO reconstructions on the short and long timescales separately because of two reasons. First, the series used to generate the long-term variations of the ENSO were also included for the generation of the short-term variations of the ENSO, such as the reconstructions by Stahle et al. (1998) and Braganza et al. (2009). Second, previous studies revealed that the ENSO agrees well with the Interdecadal Pacific Oscillation (IPO), the dominant interdecadal SST variability of the whole Pacific Ocean,

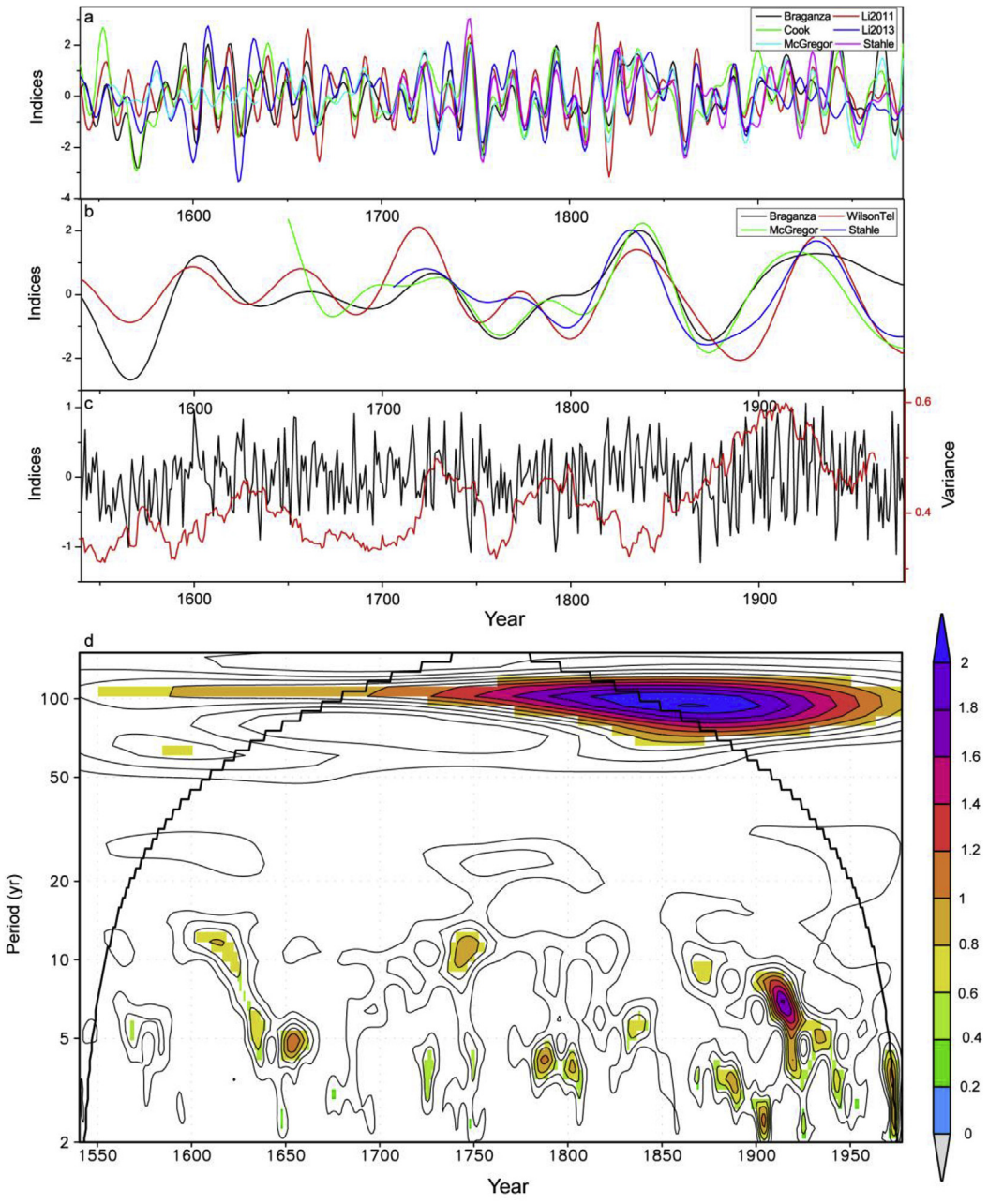

Fig. 4. Comparisons between the (a) interdecadal (10–50 years) and (b) multi-decadal (50–100 years) variations of the El Niño-Southern Oscillation (ENSO) reconstructions, the (c) synthesized ENSO reconstruction and its running variance based on a 31-year window, as well as (d) its wavelet spectrum. Insignificant periodicity in the wavelet spectrum is left empty. The codes of the reconstructions are shown in Table 1.

on both interannual and interdecadatal timescales (Fang et al., 2018a, 2018b). Since the long-term variations of the ENSO can represent large-scale interdecadal variations of the Pacific Ocean, it is reasonable to use the long-term variations ENSO reconstruction based on proxies from different locations of the Pacific Ocean to represent its long-term variability. We did not show the visual comparisons between the short-term variations in Fig. 4 because they are too compressed. Instead, the high correlations between the interannual variations of the ENSO reconstructions were illustrated in the correlation analyses above. The synthesized ENSO series showed significant correlations with the core areas of the ENSO (Fig. S4), suggesting its robustness in representing ENSO variability.

The synthesized ENSO reconstruction starts from 1540 onwards (Fig. 4c). The variance of the reconstruction generally increases since the LIA towards present (Fig. 4c). Previous studies also indicated an enhancement of the interannual variability of the ENSO in the ~20th century (Li et al., 2011; Liu et al., 2017; Stahle et al., 1998). The synthesized ENSO reconstruction shows strong periodicity on interannual and multi-decadal timescales (Fig. 4d). The interannual periodicity is most pronounced in the 20th century (Fig. 4d). The multi-decadal periodicity is the most conspicuous from 1750 onwards, with a peak at ~1860.

4. PDO

4.1. PDO reconstructions

The PDO is an ENSO-like dominant interdecadal and multi-decadal climate variability in the North Pacific Ocean (Mantua and Hare, 2002; Mantua et al., 1997; Zhang et al., 1997). The PDO is also considered as the low-frequency component of the ENSO (Mantua et al., 1997; Zhang et al., 1997). It was defined as the

Table 3
Metadata of the reconstructed Pacific Decadal Oscillation (PDO) by Biondi et al. (2001) (Biondi), D'Arrigo et al. (2001), (D'Arrigo et al., 2001), MacDonald and Case (2005), (MacDonald), D'Arrigo and Wilson (2006), (D'Arrigo, 2006), and Shen et al. (2006) (Shen). Detailed reconstructions on these reconstructions were seen in the Appendix (Descriptions of the PDO reconstructions).

Code	Var.	Data source	Exp. var.	Method	Span	Reference
Biondi	year	California and Mexico	41%	PC1	1661–1991	Biondi et al. (2001)
D'Arrigo 2001	year	Alaska, NW Canada, NW USA and Mexico	53%	PC1	1700–1979	D'Arrigo et al. (2001)
MacDonald	year	California and Alberta	45%	Linear regression	993-1996	MacDonald and Case (2005)
D'Arrigo 2006	Mar.–May	Siberia, Mongolia, Japan and Bhutan	47%	PC1	1565–1988	D'Arrigo and Wilson (2006)
Shen	year	Eastern China	78%	partial least squares regression	1470–2000	Shen et al. (2006)

dominant SST mode of northern Pacific Ocean (northern of 20°N) with its positive (negative) phase represented by the positive (negative) SST anomalies in the eastern rim of Pacific Ocean (Mantua and Hare, 2002). It has strong influence on climate change over both western North America and eastern Asia (Zhang et al., 2018). The major difference between the PDO and the ENSO is that the dominant signal for the PDO is located in the northern Pacific Ocean.

As shown in Fig. 1 and Table 3, the PDO reconstructions used in this reconstruction include three from tree rings in North America (Biondi et al., 2001; D'Arrigo et al., 2001; MacDonald and Case, 2005), two based on tree rings and historical documents from eastern Asia (D'Arrigo and Wilson, 2006; Shen et al., 2006), and one based on a global coverage of proxies (Mann et al., 2009). The reconstructions by Biondi et al. (2001) and MacDonald and Case (2005) used the tree rings from mid latitudes of western North America, while the latter one is longer and based on two tree-ring chronologies with persistent dipole changes. The reconstruction by D'Arrigo et al. (2001) not only used the tree-ring data from mid latitudes of western North America as in reconstructions by Biondi et al. (2001) and MacDonald and Case (2005), they also employed data from Alaska. The PDO were reconstructed from tree rings and historical documents by D'Arrigo et al. (2005) and Shen et al. (2006), respectively. Mann et al. (2009) constructed a global gridded temperature data set and derived a PDO reconstruction from reconstructed SST.

It is reasonable to use proxies of western North America to reconstruct the PDO because it is close to one of the two core regions of the PDO, i.e. the eastern rim of the Pacific Ocean. The PDO anomalies can modulate the temperature and precipitation of the coastal areas of western North America (Dai et al., 2015; Dong and Dai, 2015). Apart from western North America, climate in eastern Asia is also closely linked to the PDO. For example, the PDO can modulate the strength of the Asian summer monsoon (Dong and Dai, 2015). In addition, SST of the north central Pacific Ocean, one of the core areas of the PDO, is closely linked to climate in Tibetan Plateau via atmospheric circulations (Zhao et al., 2012). However, the PDO reconstruction was defined to be positive when the SST of the northern Pacific Ocean was positive (Mann et al., 2009). This definition is reverse to current definition, so we reversed the PDO reconstruction for comparisons. Detailed information on the PDO reconstructions used herein was described in the Appendix.

4.2. Synthesis of the PDO reconstructions

As shown in Table 4 the PDO reconstructions are generally poorly correlated, except for the two reconstructions by Biondi et al. (2001) and MacDonald et al. (2005). We did not calculate the correlations between the PDO reconstruction by Mann et al. (2009) and the others because the Mann et al. (2009) dataset does not have annual resolution, unlike the rest. High correlations between the two reconstructions may be because the proxies used for reconstruction were not very far from each other. Previous studies also indicated generally poor correlations between PDO reconstructions, particularly for the reconstructions using data from North America and Asia (D'Arrigo and Wilson, 2006; Kipfmueller et al., 2012). The correlations between PDO reconstructions are lower on interannual timescales but higher on long timescales. This is different from the correlations between ENSO reconstructions, which are higher on interannual timescales. This is reasonable because the PDO is more conspicuous on interdecadal and multi-decadal timescales (Mantua et al., 1997), while the ENSO has stronger signal on interannual timescales (Allan et al., 1996).

The timescale dependent correlation results are in line with the correlation analyses, and only the pairs with high correlations are shown. The PDO reconstructions by Biondi et al. (2001) and by MacDonald and Case (2005) are highly correlated, particularly on multi-decadal timescales from ~50 to 70 years (Figs. 5a and 6). Since the reconstructions by Biondi et al. (2001) and by MacDonald and Case (2005) agree well with each other and the latter one is longer, we selected the longer reconstruction by MacDonald and Case (2005) for following analyses. In addition, we found that the PDO reconstruction by MacDonald and Case (2005) shows significant correlations with the reconstruction by D'Arrigo and Wilson (2006) on multi-decadal scales at ~50 years, but their correlations are out-of-phase (Fig. 5b). As the correlations between PDO reconstructions by D'Arrigo and Wilson (2006) and MacDonald and Case (2005) are only significant on multi-decadal timescales and out-of-phase, it is not surprising that D'Arrigo and Wilson (2006) stated poor correlations with other reconstructions using proxies from North America in their original publication. Actually, for the calibration of the reconstruction by D'Arrigo and Wilson (2006), high correlation between the instrumental PDO and tree rings are mainly attributable to their good agreement on the interdecadal and multi-decadal timescales ($r = 0.70$), while the correlation between tree rings and instrumental PDO on interannual timescales is quite low ($r = 0.28$). Correlations between the other pairs of reconstructions are less significant (Fig. S5). We found that the reconstructions by MacDonald and Case (2005) and D'Arrigo and Wilson (2006) match well on multi-decadal timescales, with the reconstruction by D'Arrigo and Wilson (2006) leading by 9 years (Fig. S6). However,

Table 4
Correlations between the raw/high-passed ($f > 0.1$)/low-passed ($f < 0.1$) PDO reconstructions. The codes of the reconstructions are shown in Table 3.

	D'Arrigo2001	MacDonald	D'Arrigo2006	Shen
Biondi	0.25/0.04/0.37	0.59/0.51/0.63	0.13/0.01/0.17	0.17/0.04/0.32
D'Arrigo 2001		0.20/0.20/0.21	0.11/-0.02/0.20	0.20/0.12/0.34
MacDonald			0.06/-0.02/0.10	0.11/0.08/0.17
D'Arrigo 2006				0.16/0.09/0.26

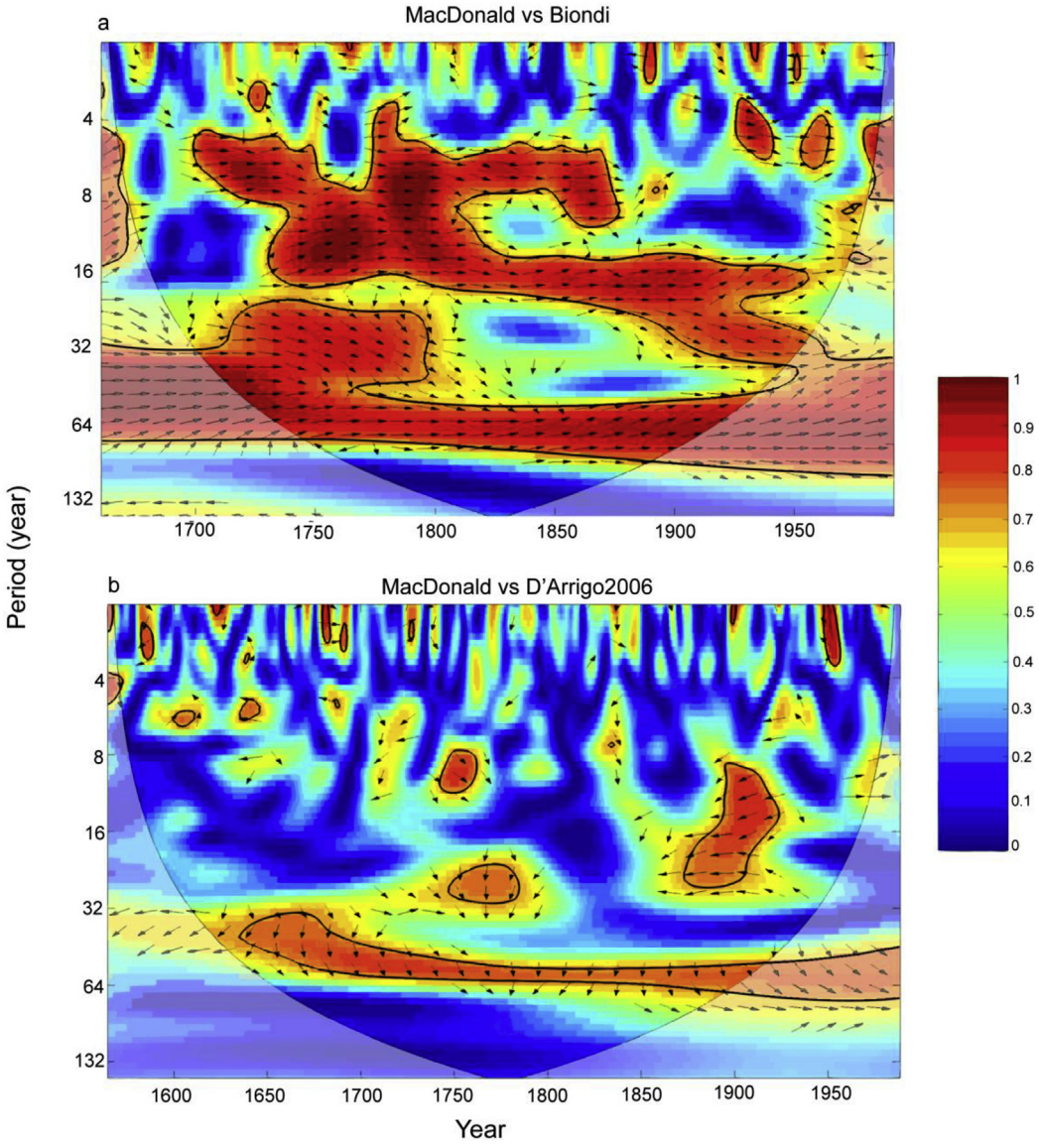

Fig. 5. Wavelet coherence (WTC) between pairs of the reconstructed Pacific Decadal Oscillation (PDO) during their common periods. The codes of the PDO reconstructions are shown in Table 3. The arrows pointing right indicate in-phase changes and pointing left indicate anti-phase changes. Significant correlations are indicated by contours and the cone of influence is shown with a narrower range at longer timescales.

regimes on the lead-lag relationships between the two PDO reconstructions remain unclear and thus the reconstruction by D'Arrigo and Wilson (2006) was not included in the synthesis.

Since the PDO reconstructions using proxies from different regions have poor matches on interannual timescales, we generated a synthesized PDO reconstruction with the interannual variability lower than 10 years removed (Fig. 7). As shown in Fig. 7a, the multi-decadal variations of the PDO reconstructions by Biondi et al. (2001) and MacDonald and Case (2005) have close agreements. A synthesized PDO reconstruction was generated by calculating the mean of the two North America reconstructions (Biondi et al., 2001; MacDonald and Case, 2005) The synthesized PDO reconstruction has the most significant multi-decadal periodicity from late 19th to the 20th centuries (Fig. 7c). The multi-decadal periodicity is moderately strong from middle 11th to 13th centuries. Its multi-decadal periodicity is particularly low from the 17th to the middle 19th centuries. The bi-decadal periodicity is relatively strong in the 11th, late 14th, early 16th, and the late 18th centuries (Fig. 7c). In general, the bi-decadal periodicity in the synthesized PDO reconstruction is less strong than the multi-decadal periodicity, which is mainly because of a weak bi-decadal periodicity in the reconstruction by MacDonald and Case (2005) (Fig. S7).

5. AMO

5.1. AMO reconstructions

The AMO is the natural variability of the dominant sea surface temperature (SST) pattern of the Atlantic Ocean (Schlesinger and Ramankutty, 1994). The positive (negative) AMO is defined as the above-average (below-average) SST averaged over the 25°-60°N, 7°-70°W region minus the global mean temperature (Schlesinger and Ramankutty, 1994). Some studies stated that the AMO is an internal process related to the Atlantic Meridional Overturning Circulation (Gray et al., 2004; Jungclaus et al., 2005), while others found linkages between the AMO and external forcings particularly after the LIA (Knudsen et al., 2014). The dominant periodicity for the AMO is 65–70 years (Schlesinger and Ramankutty, 1994).

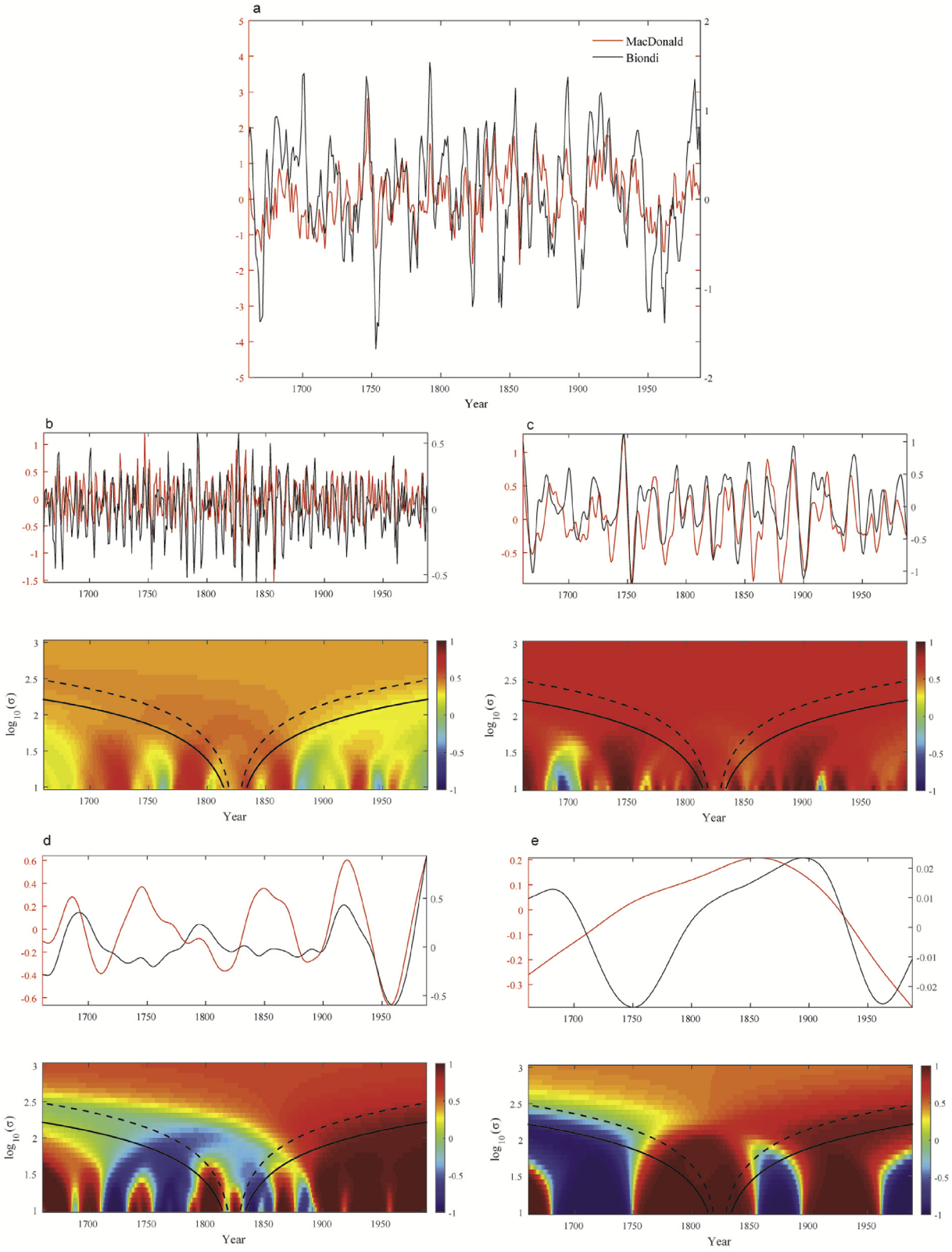

Fig. 6. Scale space correlation maps between the reconstructed Pacific Decadal Oscillation (PDO) by MacDonald and Case (2005) (MacDonald) and Biondi et al. (2001) (Biondi). The time series and the correlations from short to long timescale components were shown in consecutive panels. Introduction on the interpretation of these panels was detailed in the caption of Fig. 3.

There are four AMO reconstructions used in this work. Among them, there are two AMO reconstructions using independent proxies from northern Atlantic regions (Gray et al., 2004; Wang et al., 2017), one from northeastern Asia (Wang et al., 2011) and one based on a network of global proxies (Mann et al., 2009) (Table 5). The reconstructions by Gray et al. (2004), Wang et al. (2011) and Wang et al. (2017) have no overlapping proxies.

The AMO can influence the areas surrounding the core area of the AMO and it is straightforward to used proxy data from northern Atlantic areas for AMO reconstruction. Of the two reconstructions

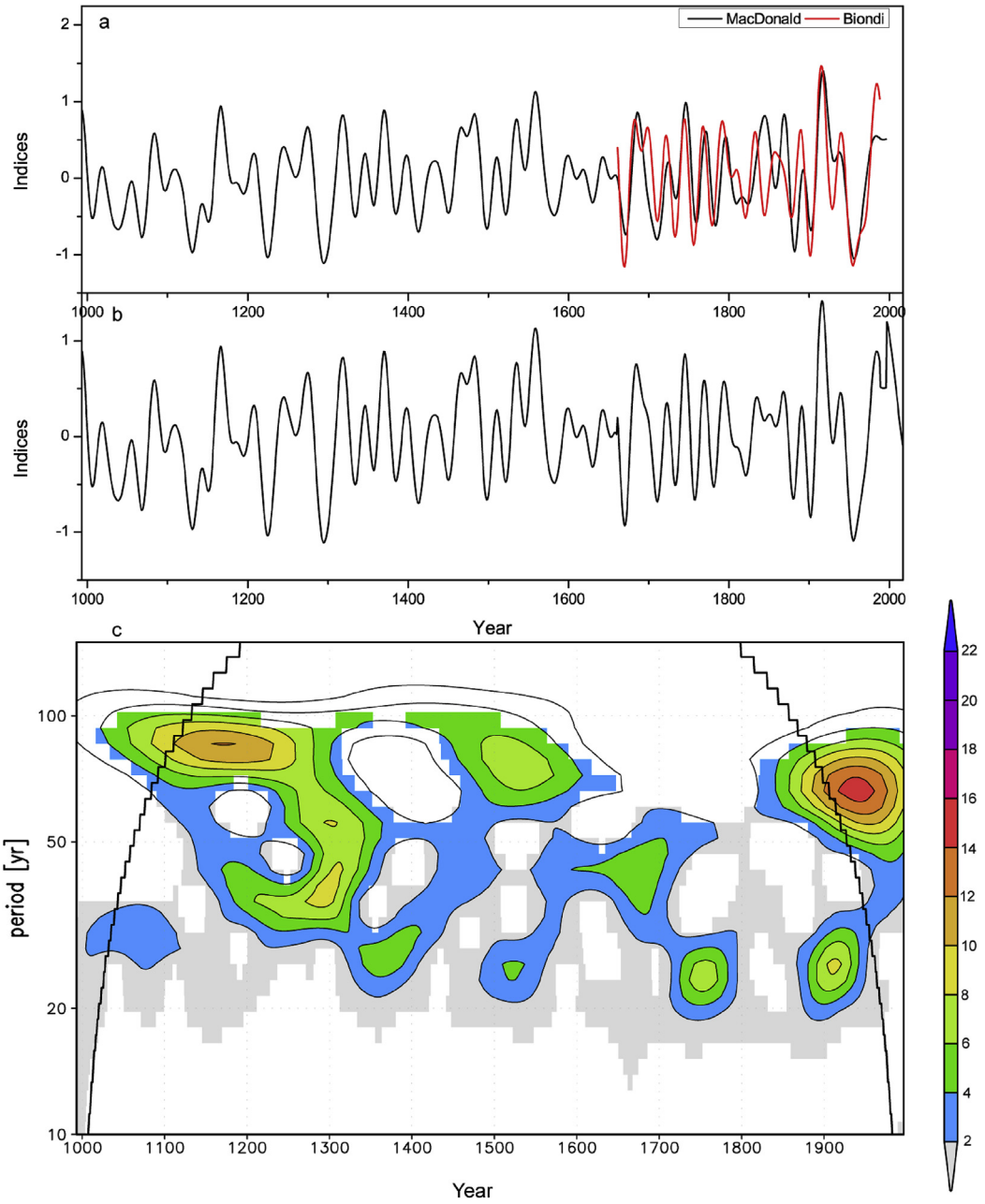

Fig. 7. Comparisons between the (a) low-frequency (20–100 years) variations of the Pacific Decadal Oscillation (PDO) reconstructions, the (b) synthesized PDO reconstruction, and (c) its wavelet spectrum. The codes of the PDO reconstructions are shown in Table 3.

Table 5
Metadata of the reconstructed Atlantic Multi-decadal Oscillation (AMO) by Gray et al. (2004) (Gray), Mann et al. (2009) (Mann), Wang et al. (2011) (Wang 2011) and Wang et al., (2017) (Wang 2017). Detailed descriptions on these reconstructions were seen in the Appendix (entitled as "Descriptions of the AMO reconstructions").

Code	Var.	Data source	Exp. var.	Method	Span	Reference
Gray	year	Southeastern America, southern Europe, Scandinavia, and Middle East	66%	4 PCs	1567–1990	Gray et al. (2004)
Mann	year	Global coverage	N/A	RegEM	500–2005	Mann et al. (2009)
Wang2011	year	Northeastern Asia	49%	PC1	1568–2009	Wang et al. (2011)
Wang2017	summer	Pan-Atlantic (northern of 20 °N)	45%	Eigen value > 1	800–2010	Wang et al. (2017)

using proxies from north Atlantic regions, the reconstruction by Gray et al. (2004) was based only on tree rings, while the reconstruction by Wang et al. (2017) included several proxies, including tree rings. Proxy data of the two reconstructions are independent. In addition, the AMO can cause climate anomalies over much of the northern hemisphere via modulating the westerlies and the Rossby wave. For example, during the warm phase of the AMO, the low surface pressures in the Atlantic areas can extend to eastern Asia and cause a weak Siberia High, resulting in a weak Asian winter monsoon and a strengthened Asian summer monsoon (Fang et al., 2018c; Wang et al., 2014). This can be associated with warm conditions over much of eastern Asia and a wet northeastern Asia. Accordingly, tree-

Table 6
Correlations between the raw/high-passed (f > 0.1)/low-passed (f < 0.1) Atlantic Multi-decadal Oscillation (AMO) reconstructions. Codes of the reconstructions are shown in Table 5.

	Wang2011	Wang2017
Gray	0.25/0.10/0.34	0.31/0.06/0.46
Wang 2011		0.22/0.01/0.39

ring data of northeastern Asia were used to reconstruct the AMO by Wang et al. (2011). Similar to the PDO reconstructions by Mann et al. (2009), they also produced an AMO reconstruction from their gridded temperature reconstructions. More descriptions of the AMO reconstructions were seen in the Appendix.

5.2. Synthesis of the AMO reconstructions

As the AMO reconstruction by Mann et al. (2009) has a different temporal resolution than other reconstructions, we did not calculate Pearson correlations with this reconstruction. As shown in Table 6, the three AMO reconstructions have almost no correlation on interannual timescales. The correlations on longer timescales are stronger, with high correlations between the AMO reconstructions by Gray et al. (2004) and Wang et al. (2017), both of which were based on proxies of the northern Atlantic areas. The correlations were more significant on long than short timescales even after accounting for the decrease in freedom due to low-pass filtering using the Chelton methods (Pyper and Peterman, 1998). The closer matches at longer scales than shorter scales in the AMO reconstructions are perhaps to be expected because the AMO mainly modulates multi-decadal climate variability. Interannual variations of the two reconstructions using proxies in the northern Atlantic areas by Gray et al. (2004) and Wang et al. (2017) have limited similarities, indicating that the interannual variability of the AMO cannot result in coherent variations even in the nearby northern Atlantic areas.

The WTC analyses supports that all the four AMO reconstructions have significant correlations but only on multi-decadal and centennial timescales (Fig. 8). The broad agreement of AMO reconstructions on multi-decadal timescales is in line with the findings that AMO can cause large-scale climate changes, including the northern Atlantic areas and the Asia (Li and Bates, 2007; Schlesinger and Ramankutty, 1994). These reconstructions have significant correlations on multi-decadal scales from ~65 to 90 years (Fig. 8). The multi-decadal correlations are generally weakened from ~1750 to 1800 (Fig. 8). During this period, a shift from coherent variations from ~90 years to ~60 years is seen. Strong correlations

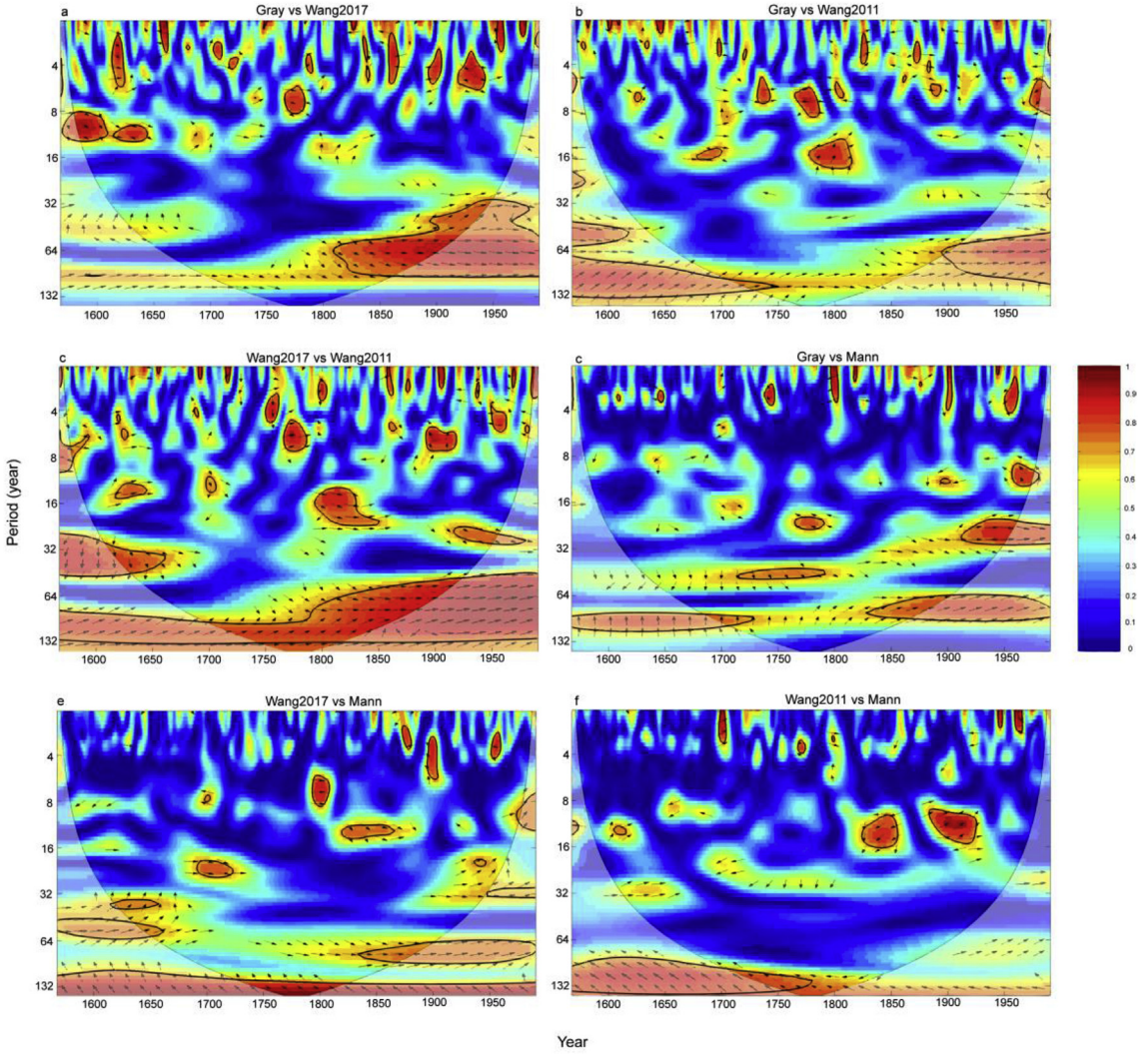

Fig. 8. Wavelet coherence (WTC) between pairs of the reconstructed Atlantic Multi-decadal Oscillation (AMO) during their common periods. The codes of the PDO reconstructions are shown in Table 5. The arrows pointing right indicate in-phase changes and pointing left indicate anti-phase changes. Significant correlations are indicated by contours and the cone of influence is shown with a narrower range at longer timescales.

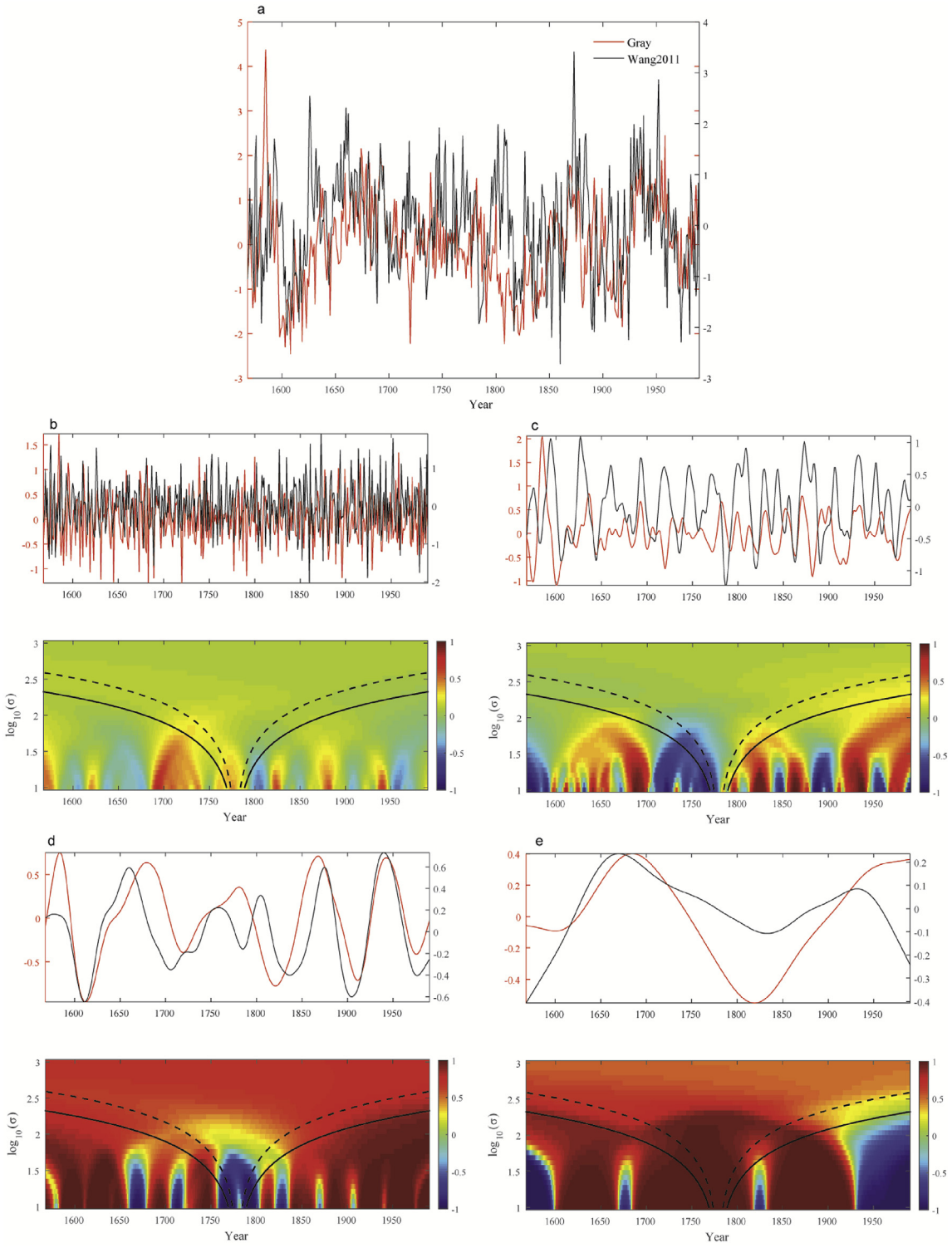

Fig. 9. Scale space correlation maps between the reconstructed Atlantic Multi-decadal Oscillation (AMO) by Gray et al. (2004) (Gray) and Wang et al. (2011) (Wang 2011). The consecutive panels are the time series and the correlations from short to long timescales. Detailed introduction on the interpretation of these panels was seen in the caption of Fig. 3.

over multi-decadal timescales for the AMO reconstructions differ from the PDO reconstructions with high correlations on inter-decadal timescales. This is reasonable since the PDO has both bi-decadal and multi-decadal periodicities and the AMO mainly has multi-decadal periodicities. To further investigate the timescale dependent correlations between reconstructions based on proxies of remote areas, we calculated the scale space correlations between the reconstructions by Gray et al. (2004) and Wang et al. (2011) based on tree rings from two sides of the Eurasian continent. As shown in Fig. 9, the two reconstructions have close matches on multi-decadal timescales, which agree with the above findings. This suggests the robust linkages between climate in northeastern Asia and the AMO on multi-decadal scales. In addition, it may also be possible that tree rings in both areas are sensitive to temperature and temperature variations are coherent over large areas of the northern hemisphere (PAGES 2k Consortium, 2013).

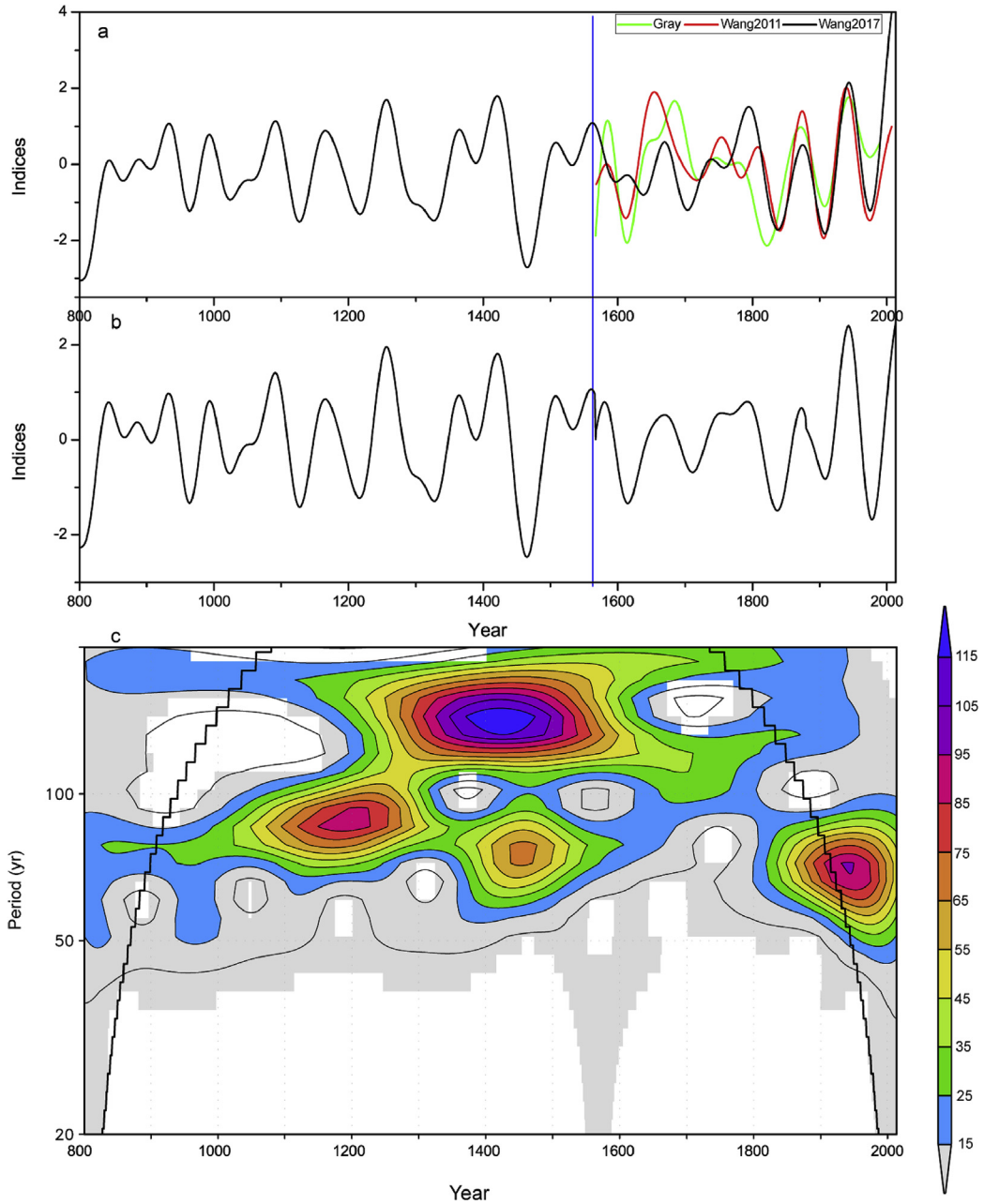

Fig. 10. Comparisons between the (a) multi-decadal (50–100 years) variations of the Atlantic Multi-decadal Oscillation (AMO) reconstructions, the (b) synthesized AMO reconstruction, and (c) its wavelet spectrum. The codes of the AMO reconstructions are shown in Table 5.

Since different AMO reconstructions have coherent variations only on multi-decadal timescales, we only retained the multi-decadal variations of the AMO reconstructions for following analyses. As shown in Fig. 10a, the multi-decadal variations of the AMO reconstructions by Gray et al. (2004), Wang et al. (2011) and Wang et al. (2017) have close matches with each other. We first averaged the two reconstructions based on proxies from northern Atlantic areas (Gray et al., 2004; Wang et al., 2017), which were then averaged with the reconstruction using proxies from eastern Asia (Wang et al., 2011) to produce the synthesized reconstruction (Fig. 10b). This is to avoid overweighting the reconstructions using proxies of Atlantic areas relative to the one using the proxies of eastern Asia. The synthesized AMO reconstruction shows largest amplitude in the early 15th century (Fig. 10b), which correspond to a strong centennial periodicity (Fig. 10c). The multi-decadal periodicity is pronounced in the 12th, 16th and from late 19th to 20th centuries (Fig. 10c). A strongest multi-decadal periodicity is seen in the 20th century. Multi-decadal periodicity of the AMO is low from the 9th to 10th centuries and the 18th century.

6. Responses of oceanic and atmospheric modes to solar irradiation

With these synthesized reconstructions, we studied the responses of climate modes of the Pacific and Atlantic Oceans to solar irradiation. The PDO generally agree with the ENSO particularly when their bi-decadal variability was enhanced in the 18th century (Fig. S8). Since the ENSO modulates both the interannual, inter-decadal and multi-decadal climate variability of the whole Pacific areas (Allan et al., 1996; Fang et al., 2018a). Thus we used the AMO

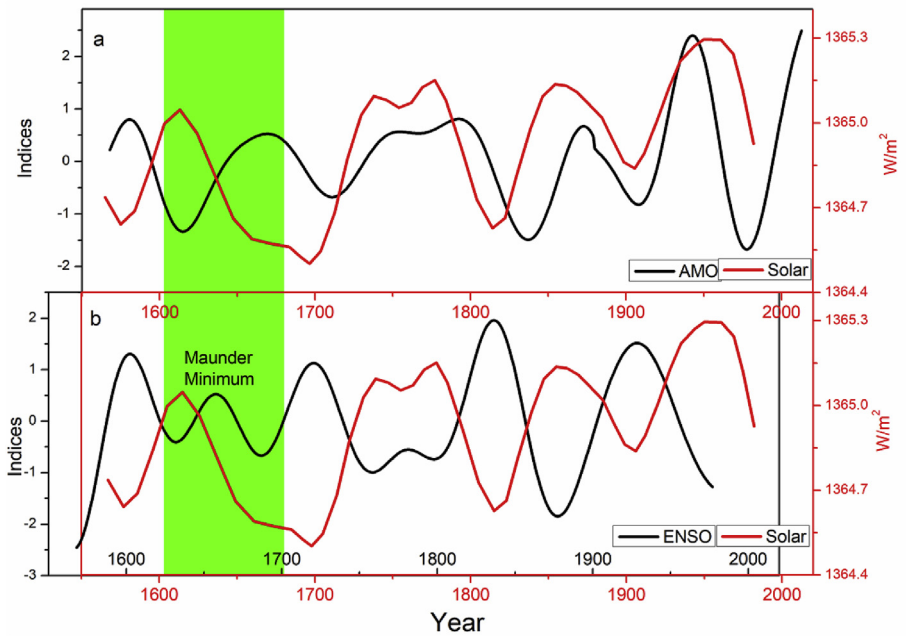

Fig. 11. Comparisons between the multi-decadal variations of the solar irradiation and (a) the synthesized reconstructions of the Atlantic Multi-decadal Oscillation (AMO), and the (b) El Niño-Southern Oscillation (ENSO). The reconstructed ENSO has been lagged for about 20 years.

and ENSO to represent the climate variability of Atlantic and Pacific Oceans. As the synthesized AMO reconstruction only contains multi-decadal variability, the comparisons were only implemented on multi-decadal scales (Eddy, 1976).

From the Maunder Minimum from 1645 to 1715 (Eddy, 1976) to the 20th century, the AMO appears to have a prompt and positive response to the solar irradiation (Fig. 11a). This agrees with the previous findings based on comparisons between solar irradiation and the AMO reconstruction by Gray et al. (2004) (Knudsen et al., 2014), which has similar multi-decadal variations with our synthesized AMO reconstruction (Fig. 10). Previous study revealed that their correlations were highly significant on multi-decadal timescales comparing with the 10,000 randomly generated red-noise data (Knudsen et al., 2014). Our comparisons generally agree with this previous study, suggesting that the solar activities play a dominant role pacing the AMO after the Maunder Minimum. Modeling studies indicated that enhanced solar irradiance can strengthen the Atlantic Meridional Overturning Circulation and cause a positive phase of the AMO in a prompt way (Seidenglanz et al., 2012).

On the other hand, multi-decadal variations of the ENSO showed a negative response to solar irradiation lagging about 20 years (Fig. 11b). A negative response to solar irradiation was widely reported in previous studies. Modeling studies evidenced a negative phase of the ENSO in response to an enhanced solar irradiation (Liu et al., 2013). A reconstruction based on globally distributed proxy data also supports a negative phase of ENSO during the solar forced warm period (Mann et al., 2009). A negative phase of ENSO is in general followed by an enhanced Asian summer monsoon (Liu et al., 2013). A lagged response of PDO to AMO was revealed in previous study (D'Orgeville and Peltier, 2007). The AMO changes can force Pacific SST anomalies via atmospheric circulations (D'Orgeville and Peltier, 2007; Sun et al., 2017).

7. Conclusions

Different ENSO reconstructions have close matches on from interannual to multi-decadal timescales, while the PDO and AMO reconstructions only have close matches on interdecadal and multi-decadal timescales. The interannual and interdecadal variations of the synthesized ENSO reconstruction are based on all the existing reconstructions, except for the reconstructions by Wilson et al. (2010). The multi-decadal variations of the synthesized ENSO reconstruction are produced as the mean of the reconstructions by Stahle et al. (1998), Braganza et al. (2009), Wilson et al. (2010) and McGregor et al. (2010). A synthesized multi-decadal PDO reconstruction was produced as the average of the reconstructions by Biondi et al. (2001) and MacDonald and Case (2005) A synthesized multi-decadal AMO reconstruction was constructed as the average of the reconstructions by Gray et al. (2004), Wang et al. (2011) and Wang et al. (2017).

The interannual variability and periodicity of the ENSO are most pronounced in the 20th century. Both of the PDO and AMO exhibit the strongest multi-decadal periodicity from late 19th to the 20th centuries. On multi-decadal timescales, after the Maunder Minimum period, the AMO was promptly and positively responded to solar irradiation, while the ENSO showed a negative response to solar irradiation with a lag of ~20 years. This study is the first attempt to catalogue and compare reconstructed major modes of the Pacific and Atlantic Oceans. We are encouraged by being able to extract some robust long-term behavior of climate signals via comparisons of these reconstructions. At the same time, our study brings light to many remaining challenges and research priorities to more accurately address the climate system. Addressing these challenges is particularly important as the long-term dynamics of the oceanic and atmospheric modes are primarily responsible for climate changes on societally relevant timescales and politically relevant spatial scales.

Acknowledgements

We acknowledge the authors who have contributed their data to make this study possible. The constructive remarks and suggestions from two anonymous reviewers are highly appreciated. This study was funded by the Strategic Priority Research Program of Chinese Academy of Sciences (XDB26020000), Excellent Youth Fund of the

National Science Foundation of China (41822101), fellowship for the National Youth Talent Support Program of China (Ten Thousand People Plan), fellowship for Youth Talent Support Program of Fujian Province and the innovation team project (IRTL1705). Supports from the Swedish VR, Formas (Future Research Leaders), VINNOVA, STINT, BECC, MERGE, SNIC through S-CMIP, and the Academy of Finland (EBOR and GRASS projects) are also acknowledged.

Appendix A. Supplementary data

Supplementary data to this article can be found online at https://doi.org/10.1016/j.quascirev.2019.05.014.

References

Allan, R., Lindesay, J., Parker, D., 1996. El Nino: Southern Oscillation and Climatic Variability. CSIRO, Australia.
Biondi, F., Gershunov, A., Cayan, D.R., 2001. North Pacific decadal climate variability since 1661. J. Clim. 14, 5–10.
Braganza, K., Gergis, J.L., Power, S.B., Risbey, J.S., Fowler, A.M., 2009. A multiproxy index of the El Niño–southern oscillation, A.D. 1525–1982. J. Geophys. Res. Atmos. 114, D05106–D05122.
Chaudhuri, P., Marron, J.S., 1999. Sizer for Exploration of Structures in Curves, vol. 94. Publications of the American Statistical Association, pp. 807–823.
Cook, E., D'Arrigo, R., Anchukaitis, K., 2008. ENSO Reconstructions from Long Tree-Ring Chronologies: Unifying the Differences, Talk Presented at a Special Workshop on Reconciling ENSO Chronologies for the Past.
Cook, E., Woodhouse, C.A., Eakin, C.M., Meko, D.M., Stahle, D.W., 2004. Long-term aridity changes in the western United States. Science 306, 1015.
Cook, E.R., D'Arrigo, R.D., Mann, M.E., 2002. A well-verified, multiproxy reconstruction of the winter North Atlantic Oscillation Index since ad 1400. J. Clim. 15, 1754–1764.
D'Arrigo, R., Cook, E.R., Wilson, R.J., Allan, R., Mann, M.E., 2005. On the variability of ENSO over the past six centuries. Geophys. Res. Lett. 32, 321–336.
D'Arrigo, R., Villalba, R., Wiles, G., 2001. Tree-ring estimates of Pacific decadal climate variability. Clim. Dyn. 18, 219–224.
D'Arrigo, R., Wilson, R., 2006. On the Asian expression of the PDO. Int. J. Climatol. 26, 1607–1617.
D'Orgeville, M., Peltier, W.R., 2007. On the Pacific decadal oscillation and the Atlantic multidecadal oscillation: might they be related? Geophys. Res. Lett. 34, 298–318.
Dai, A., Fyfe, J.C., Xie, S.P., Dai, X., 2015. Decadal modulation of global surface temperature by internal climate variability. Nat. Clim. Change 5. https://doi.org/10.1038/NCLIMATE2605.
Dong, B., Dai, A., 2015. The influence of the interdecadal Pacific oscillation on temperature and precipitation over the globe. Clim. Dyn. 45, 2667–2681.
Eddy, J.A., 1976. The maunder minimum. Science 192, 1189–1202.
Fang, K., Chen, D., Ilvonen, L., Frank, D., Pasanen, L., Holmström, L., Zhao, Y., Zhang, P., Seppä, H., 2018a. Time-varying relationships among oceanic and atmospheric modes:A turning point at around 1940. Quat. Int. 487, 12–25.
Fang, K., Cook, E., Guo, Z., Chen, D., Ou, T., Frank, D., Zhao, Y., 2018b. Synchronous multi-decadal tree-ring patterns of the Pacific areas reveal dynamics of the Interdecadal Pacific Oscillation (IPO) since 1567. Environ. Res. Lett. https://doi.org/10.1088/1748-9326/aa9f74.
Fang, K., Guo, Z., Chen, D., Wang, L., Dong, Z., Zhou, F., Zhao, Y., Li, J., Li, Y., Cao, X., 2018c. Interdecadal modulation of the Atlantic Multi-decadal Oscillation (AMO) on southwest China's temperature over the past 250 years. Clim. Dyn. https://doi.org/10.1007/s00382-00018-04244-x.
Fang, K., Seppä, H., Chen, D., 2014. Interdecadal hydroclimate teleconnections between Asia and North America over the past 600 years. Clim. Dyn. 7–8, 1777–1787.
Gergis, J.L., Fowler, A.M., 2009. A history of ENSO events since A.D. 1525: implications for future climate change. Clim. Change 92, 343–387.
Ghil, M., Allen, M.R., Dettinger, M.D., Ide, K., Kondrashov, D., Mann, M.E., Robertson, A.W., Saunders, A., Tian, Y., Varadi, F., 2002. Advanced spectral methods for climatic time series. Rev. Geophys. 40, 1003 doi: 1010.1029/2000RG000092.
Gray, S.T., Graumlich, L.J., Betancourt, J.L., Pederson, G.T., 2004. A tree-ring based reconstruction of the Atlantic Multidecadal Oscillation since 1567 AD. Geophys. Res. Lett. 31, L12205. DOI: 12210.11029/12004GL019932.
Grinsted, A., Moore, J.C., Jevrejeva, S., 2004. Application of the cross wavelet transform and wavelet coherence to geophysical time series. Nonlinear Process Geophys. 11, 561–566.
Holmström, L., Pasanen, L., 2017. Statistical scale space methods. Int. Stat. Rev. 85, 1–30.
Jungclaus, J.H., Haak, H., Latif, M., Mikolajewicz, U., 2005. Arctic-North Atlantic interactions and multidecadal variability of the meridional overturning circulation. J. Clim. 18, 4013–4031.
Kipfmueller, K.F., Larson, E.R., St George, S., 2012. Does proxy uncertainty affect the relations inferred between the Pacific Decadal Oscillation and wildfire activity in the western United States? Geophys. Res. Lett. 39 https://doi.org/10.1029/2011GL050645.
Knudsen, M.F., Jacobsen, B.H., Seidenkrantz, M.-S., Olsen, J., 2014. Evidence for external forcing of the Atlantic multidecadal oscillation since termination of the Little Ice Age. Nat. Commun. 5 https://doi.org/10.1038/ncomms4323.
Li, J., Xie, S.P., Cook, E., Morales, M.S., Christie, D.A., Johnson, N.C., Chen, F., D'Arrigo, R., Fowler, A.M., Gou, X., Fang, K., 2013. El Niño modulations over the past seven centuries: amplitude, teleconnection, and the volcanic effect. Nat. Clim. Change 3. https://doi.org/10.1038/NCLIMATE1936.
Li, J., Xie, S.P., Cook, E.R., Huang, G., D'Arrigo, R., Liu, F., Ma, J., Zheng, X.T., 2011. Interdecadal modulation of El Nino amplitude during the past millennium. Nat. Clim. Change 1, 114–118.
Li, S., Bates, G.T., 2007. Influence of the Atlantic multidecadal oscillation on the winter climate of East China. Adv. Atmos. Sci. 24, 126–135.
Liu, J., Wang, B., Cane, M.A., Yim, S.-Y., Lee, J.-Y., 2013. Divergent global precipitation changes induced by natural versus anthropogenic forcing. Nature 493, 656–659.
Liu, Y., Cobb, K.M., Song, H., Li, Q., Li, C.Y., Nakatsuka, T., An, Z., Zhou, W., Cai, Q., Li, J., 2017. Recent enhancement of central Pacific El Niño variability relative to last eight centuries. Nat. Commun. 8, 15386. DOI: 15310.11038/ncomms15386.
MacDonald, G.M., Case, R.A., 2005. Variations in the Pacific decadal oscillation over the past millennium. Geophys. Res. Lett. 32, L08703 doi:08710.01029/02005GL022478.
Mann, M.E., Zhang, Z., Rutherford, S., Bradley, R.S., Hughes, M.K., Shindell, D., Ammann, C., Faluvegi, G., Ni, F., 2009. Global signatures and dynamical origins of the Little Ice Age and medieval climate anomaly. Science 326, 1256–1260.
Mantua, N.J., Hare, S.R., 2002. The Pacific decadal oscillation. J. Oceanogr. 58, 35–44.
Mantua, N.J., Hare, S.R., Zhang, Y., Wallace, J.M., Francis, R.C., 1997. A Pacific interdecadal climate oscillation with impacts on salmon production. Bull. Am. Meteorol. Soc. 78, 1069–1079.
McGregor, S., Timmermann, A., Timm, O., 2010. A unified proxy for ENSO and PDO variability since 1650. Clim. Past 6, 1–17.
PAGES 2k Consortium, 2013. Continental-scale temperature variability during the past two millennia. Nat. Geosci. 6, 339–346.
Park, J., 1992. Envelope estimation for quasi-periodic geophysical signals in noise: a multitaper approach. Stat. Environ. Earth Sci. 189, C219.
Pasanen, L., Holmström, L., 2017. Scale space multiresolution correlation analysis for time series data. Comput. Stat. 31, 197–218.
Pyper, B.J., Peterman, R.M., 1998. Comparison of methods to account for autocorrelation in correlation analyses of fish data. Can. J. Fish. Aquat. Sci. 55, 2127–2140.
Schlesinger, M.E., Ramankutty, N., 1994. An oscillation in the global climate system of period 65-70 years. Nature 367, 723–726.
Seidenglanz, A., Prange, M., Varma, V., Schulz, M., 2012. Ocean temperature response to idealized Gleissberg and de Vries solar cycles in a comprehensive climate model. Geophys. Res. Lett. 39, L22602.
Shen, C., Wang, W.C., Gong, W., Hao, Z., 2006. A Pacific Decadal Oscillation record since 1470 AD reconstructed from proxy data of summer rainfall over eastern China. Geophys. Res. Lett. 33, L03702.
Stahle, D.W., Cleaveland, M., Therrell, M., Gay, D., D'arrigo, R., Krusic, P., Cook, E., Allan, R., Cole, J., Dunbar, R., 1998. Experimental dendroclimatic reconstruction of the southern oscillation. Bull. Am. Meteorol. Soc. 79, 2137–2152.
Stocker, T.F., Qin, D., Plattner, G., Tignor, M., Allen, S., Boschung, J., Nauels, A., Xia, Y., Bex, V., Midgley, P., 2013. Climate Change 2013: the Physical Science Basis. Intergovernmental Panel on Climate Change, Working Group I Contribution to the IPCC Fifth Assessment Report (AR5). Cambridge University Press, New York.
Sun, C., Kucharski, F., Li, J., Jin, F., Kang, I., Ding, R., 2017. Western tropical Pacific multidecadal variability forced by the Atlantic multidecadal oscillation. Nat. Commun. 8, 15998. https://doi.org/10.1038/ncomms15998.
Torrence, C., Compo, G.P., 1998. A practical guide to wavelet analysis. Bull. Am. Meteorol. Soc. 79, 61–78.
Villalba, R., Lara, A., Masiokas, M.H., Urrutia, R., Luckman, B.H., Marshall, G.J., Mundo, I.A., Christie, D.A., Cook, E.R., Neukom, R., 2012. Unusual southern hemisphere tree growth patterns induced by changes in the southern Annular mode. Nat. Geosci. 5, 793–798.
Walker, G.T., Bliss, E., 1932. World weather. V. Mem. Roy. Meteor. Soc. 4, 53–84.
Wang, J., Bao, Y., Qin, C., Kang, S., He, M., Wang, Z., 2014. Tree-ring inferred annual mean temperature variations on the southeastern Tibetan Plateau during the last millennium and their relationships with the Atlantic Multidecadal Oscillation. Clim. Dyn. 43, 627–640.
Wang, J., Yang, B., Ljungqvist, F.C., Luterbacher, J., Osborn, T., Briffa, K., Zorita, E., 2017. Internal and external forcing of multidecadal Atlantic climate variability over the past 1,200 years. Nat. Geosci. https://doi.org/10.1038/NGEO2962.
Wang, X., Brown, P.M., Zhang, Y., Song, L., 2011. Imprint of the Atlantic multidecadal oscillation on tree-ring widths in Northeastern Asia since 1568. PLoS One 6, e22740.
Wilson, R., Cook, E., D'Arrigo, R., Riedwyl, N., Evans, M.N., Tudhope, A., Allan, R., 2010. Reconstructing ENSO: the influence of method, proxy data, climate forcing and teleconnections. J. Quat. Sci. 25, 62–78.
Zhang, Y., Wallace, J.M., Battisti, D.S., 1997. ENSO-like interdecadal variability: 1900-93. J. Clim. 10, 1004–1020.
Zhang, Y., Xie, S.-P., Kosaka, Y., Yang, J.-C., 2018. Pacific decadal oscillation: tropical Pacific forcing versus internal variability. J. Clim. 31, 8265–8279.
Zhao, P., Wang, B., Zhou, X., 2012. Boreal summer continental monsoon rainfall and hydroclimate anomalies associated with the Asian-Pacific Oscillation. Clim. Dyn. 39, 1197–1207.